A Super Wideband CPW-Fed Elliptical Slot Monopole Antenna for Wireless Applications

Budhadeb Maity[1], [*] and Sisir K. Nayak[2]

Abstract—This article presents a coplanar waveguide (CPW)-fed super wideband (SWB) elliptical slot monopole (ESM) antenna for wireless applications. The SWB impedance bandwidth (IBW) is achieved by symmetrical excitation of the defective ground plane with a dodecagon-shaped annular ring (DSAR) radiator. The dimension of a prototype proposed antenna is $0.239\lambda_l \times 0.253\lambda_l \times 0.004\lambda_l$ mm^3 (λ_l corresponding to the wavelength for the lowest operational frequency). A high bandwidth ratio of approximately $16.34:1$ is produced by the combined radiation, with observed -10 dB IBW from 1.613 to 26.357 GHz (176.93%). Despite the cross-polarization levels being significantly suppressed in the H-plane, the basic concepts of an SWB antenna design have been successfully presented. Additionally, compared to other antennas mentioned in the literature, the proposed ESM antenna has a wider IBW. Successful fabrication, implementation, and comparison of the prototype with the experimental results are presented in this article.

1. INTRODUCTION

Printed microstrip slot antennas are commonly used in wireless communications systems because of their benefits, which include light weight, low profile, low cost, and simplicity of integration with monolithic microwave integrated circuits (MMICs). However, a new problem is brought about by the microstrip slot antenna's narrow bandwidth, which is essential to the quality of ultra-wideband (UWB) communications. Coplanar waveguide (CPW)-fed antennas are flexible and offer a comparatively wide bandwidth compared to microstrip-fed antennas. The fast data rates and low fading sensitivity may be integrated with surface-mount devices and used for UWB antenna operation [1, 2]. But the demand for various CPW-fed printed antennas with wider bandwidth and smaller sizes have significantly increased in current wireless communications. According to [3], the monopole and Vivaldi antennas are often employed because of their wide bandwidth and good radiation. A rather large area is needed in both situations since Vivaldi antennas need a tapered slot and monopole antennas are mounted perpendicular to carriers. The slot antenna has been improved recently to meet the need for increased impedance bandwidth (IBW). Numerous concepts with small sizes and increased bandwidth have been put forth [4–8]. To improve radiation performance similar to the monopole antenna stretches the length of the central metallic strip line beyond the CPW-fed plane [4]. Similar to how the central strip is crucial in determining the wider IBW, various shapes have been developed as a result, including CPW-fed antennas with dual-reverse-arrow fractal structures [5], flexible bow-tie slot antenna [6], rose-curve monopole antenna [7], traveling wave series-fed circular slit microstrip array [8], etc. The size of this antenna limits its ability to deliver larger IBW performance, despite its wideband fractal forms structure. Though these antennas had small sizes, the IBWs were still less than 112%.

* Corresponding author: Budhadeb Maity (maity176151008@iitg.ac.in).
[1] School of Energy Science and Engineering, Indian Institute of Technology Guwahati, Guwahati 781039, Assam, India. [2] Department of Electronics and Electrical Engineering, Indian Institute of Technology Guwahati, Guwahati 781039, Assam, India.

Recently, compactness is a key requirement for today's wireless applications, such as UWB applications, and this is motivating research into smaller circular-arc-shaped monopole arrays [9], the variation of lower and upper resonant frequency to the width of a U-slot [10], wideband fractal shapes structure [11], etc. However, the size is $2\lambda_l \times 2\lambda_l \times 0.05\lambda_l$ mm^3. For a wider bandwidth, [12] uses a central monopole meandered-slot compact antenna design. The antenna proposed in [13–15], which is different from other CPW-fed slot antennas and features a printed E-shape slot, an arc shape stub, and a fishtail shape, is utilized exclusively for stimulating the slot and has a very good IBW. The symmetrical staircase-shaped structure is used by a slotted antenna to improve the matched antenna feed and IBW [16]. Similarly, an asymmetrical ground plane, semi-elliptically fractal slot patch antenna with 172% IBW is proposed in [17]. We are inspired to design a compact wider IBW antenna in this part because the above antennas either have thick profiles or have large structures. Also, the IBW is increased while maintaining the low cross-polarization levels by employing a dodecagon-shaped annular ring radiator (DSAR).

This work presents a compact SWB elliptical slot monopole (ESM) antenna that covers the entire microwave and lower millimeter wave spectrum where the antenna is integrated into a compact SWB DSAR radiator to realize improved radiation in the desired direction. Therefore, for SWB wireless applications, this research provides a unique, compact, low-cost, straightforward design, and simple-to-build ESM antenna. The main radiator of the proposed antenna is a DSAR radiator, and it is built on a low-cost FR-4 substrate. The CPW-fed approach, which covers the measured -10 dB IBW from 1.613 to 26.357 GHz (176.93%) band with a bandwidth ratio of approximately 16.34 : 1 and significantly suppressed the cross-polarization levels in H-plane. Additionally, to confirm that the proposed ESM antenna is suitable for SWB wireless applications, simulated results validated with experimental results have been obtained.

The structure of this work is as follows. The design procedures and enhanced IBW of the proposed antenna are described in Section 2. The parametric studies and impedance matching of the antenna are presented in Section 3. In Section 4, the prototype measured and simulated results are shown and contrasted. Section 5 provides a summary of this work's conclusion.

2. METHODOLOGY

Figure 1 shows the proposed elliptical slot monopole (ESM) antenna's structural arrangement in detail. The proposed antenna is printed with a dielectric constant $(\epsilon_r) = 4.3$ and a loss tangent $(\tan\delta) = 0.025$ on a rectangular FR-4 substrate with a thickness of 0.8 mm. The CST Microwave Studio (CST vers. 17) is used for simulation work. As previously mentioned, the primary radiator is a dodecagon-shaped annular ring (DSAR) structure with an outer radius r_2 of 17.2 mm and an inner radius r_1 of 3.5 mm.
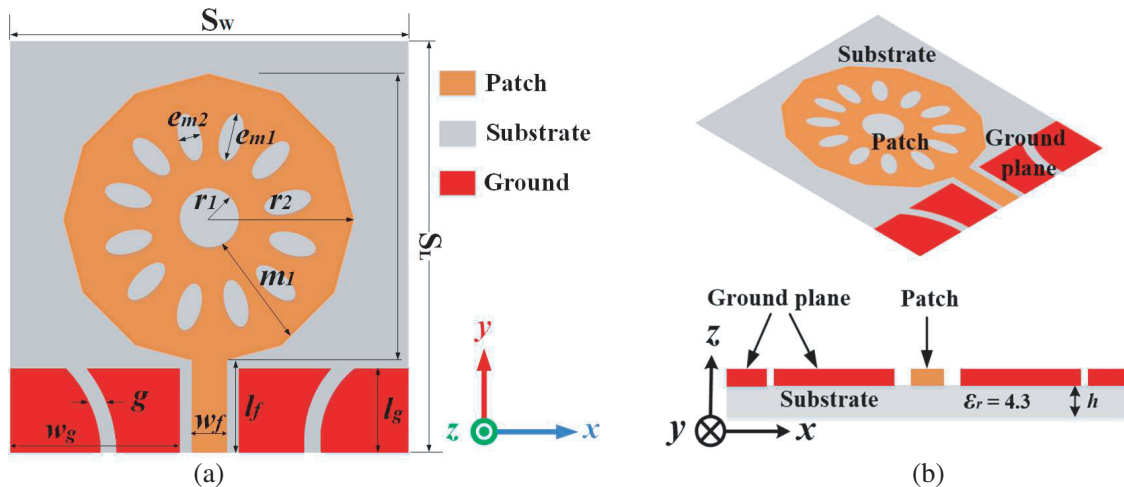

Figure 1. Propose antenna geometry. (a) Top view and (b) side view and isometric view.

Table 1. Dimensional specifications for the proposed antenna.

Parameter	Units (mm)	Parameter	Units (mm)	Parameter	Units (mm)
S_L	44.5	m_1	13.7	l_g	7.7
S_W	47.20	e_{m1}	2.8	l_f	8.8
r_1	3.5	e_{m2}	1.8	w_f	3.1
r_2	17.2	w_g	21.1	g	1.8

Additionally, 12 elliptical-shaped slots with minor and major axes of 1.8 and 2.8 mm each have been added to the primary radiator. A pair of partially circular slits are introduced on the defective ground plane, and its gap g is equal to 1.8 mm. Table 1 is a list of the DSAR radiator and defective ground plane optimal design parameters for the aforementioned antenna design. A 50 Ω microstrip line connects to the radiator. Initially, the outer radius r_2 is calculated using the Equation (2) shown below [18]:

$$f_r = \frac{1.8412 \times c}{4\pi R_e \sqrt{\epsilon_r}} \tag{1}$$

$$R_e = r_2 \left\{ 1 + \frac{2h_{FR-4}}{\pi \epsilon_r r_2} \left[\ln\left(\frac{\pi r_2}{2h_{FR-4}}\right) + 1.7726 \right] \right\}^{1/2} \tag{2}$$

$$\tag{3}$$

The inner radius r_1 is then given by

$$r_1 = \frac{R_e}{\left\{ 1 + \frac{2h_{FR-4}}{\pi \epsilon_r R_e} \left[\ln\left(\frac{\pi R_e}{2h_{FR-4}}\right) + 1.7726 \right] \right\}^{1/2}} \tag{4}$$

where R_e is the effective outer radius of the radiator, and f_r, h_{FR-4}, and ϵ_r denote the central resonance frequency, substrate thickness, and substrate permittivity, respectively. The outer radius r_2 is evaluated using Equation (2) at the lower resonant frequencies f_{lr} of 2.4 GHz to support TM_{11} mode [19].

2.1. Design Evolution

Figure 2 shows the evolution of the ESM CPW-fed antenna's design and the corresponding performance of the reflection coefficient S_{11}. Prototype-A, a simple DSAR radiator with a CPW-fed planar antenna [20] that can give one wider and another narrow -10 dB IBW performance but cannot provide a wideband frequency operation with perfect impedance matching, is depicted in Figure 2(b). However, due to its limited -10 dB IBW from 2.45 to 23.50 GHz, it is unable to cover all UWB frequency bands. The second step is improvised, in which 12 elliptical-shaped slots on the main radiator are introduced within the DSAR structure, without disturbing the proposed antenna's compactness. This is done to further improve the impedance matching of this exciting resonance frequency. Its associated S_{11} performance explains that a well-improved -10 dB IBW of 2.12–23.56 GHz is reached. However, the second step's improvement in matching is still insufficient to cover the wider bands of interest. Therefore, to further enhance the operating bandwidth, a third step is introduced, in which one pair of partially circular slits are introduced into the CPW-fed ground plane, and its gap $g = 1.8$ mm. Notably, this introduced partially circular slits in the third step has aided in increasing the very wide -10 dB IBW of 174.61% due to the etched two slits, adding a new SWB mode. The additional SWB frequency can be adjusted by varying the major and minor axes of 2.8 mm and 1.8 mm, respectively. The wider first and second bands are chosen to overlap to provide a continuous wider band that covers the SWB frequency ranging from 1.902 GHz to 28.067 GHz (174.61%).

Figures 3(a)–3(f) illustrate the study of the simulated surface current distributions for the proposed antenna at various frequencies, which are 2.41, 5.92, 8.86, 10.91, 18.33, and 22.98 GHz, respectively. The majority of the surface currents in Figures 3(a)–3(b) are localized close to the radiator's fed and feeding points. Similarly, the majority of the surface currents are centered close to the fed and edge
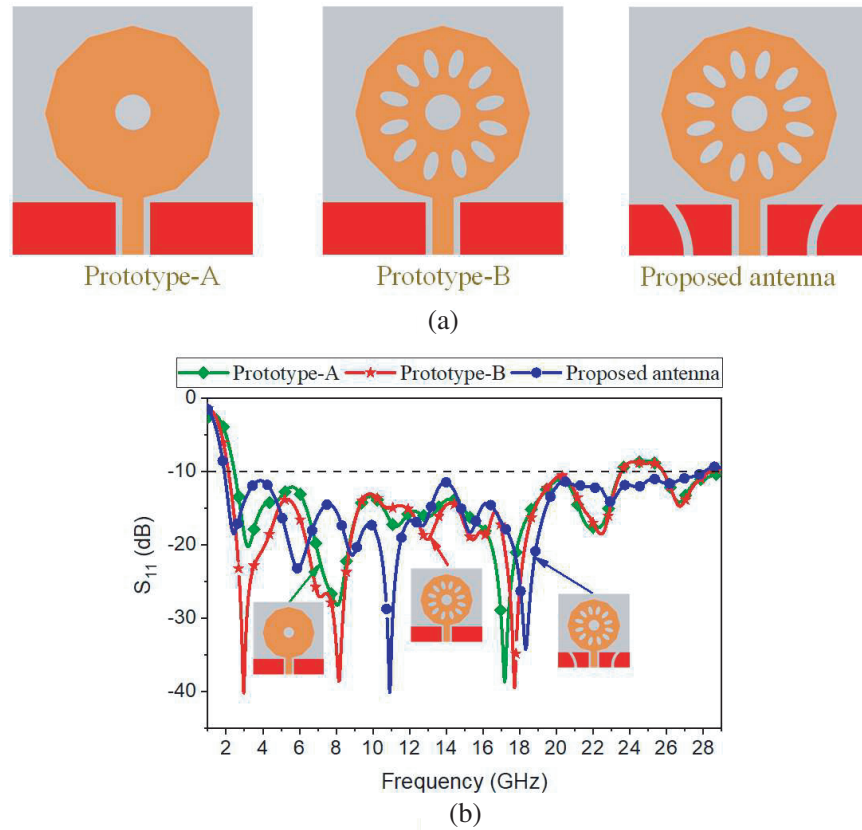
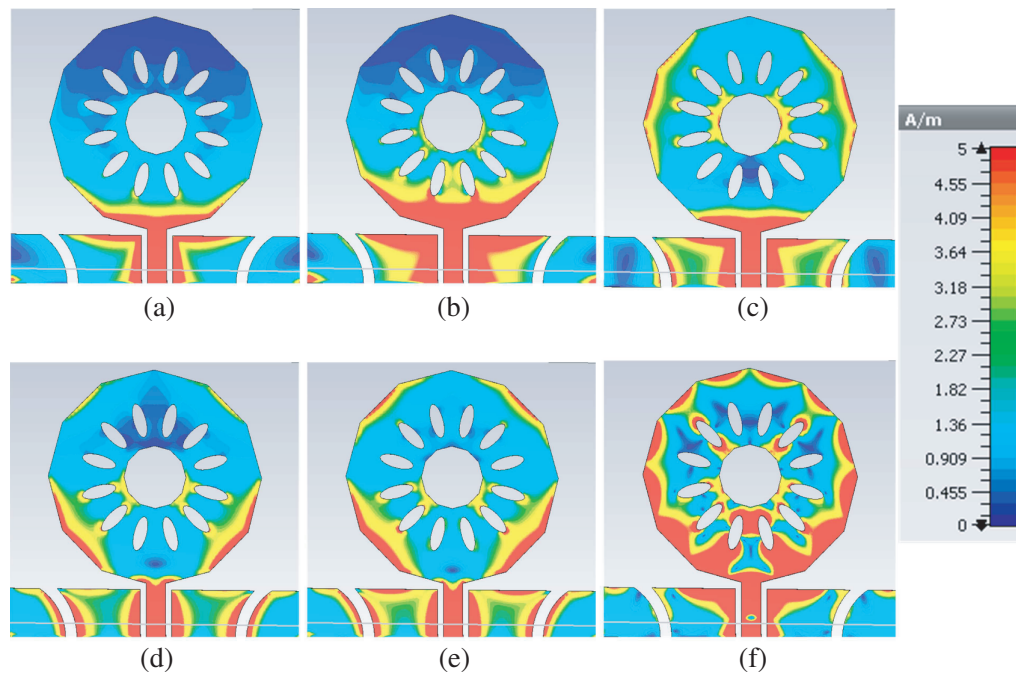**Figure 2.** (a) Design evolution of the proposed antenna and (b) corresponding simulated S_{11}.

Figure 3. Simulated surface current distributions of the proposed antenna for (a) 2.41 GHz, (b) 5.92 GHz, (c) 8.86 GHz, (d) 10.91 GHz, (e)18.33 GHz, and (f) 22.98 GHz.

of the annular ring radiator in Figures 3(c)–3(e). The current distribution at 22.98 GHz is shown in Figure 3(f), where larger surface currents are concentrated close to the edge of the DSAR radiator.

The simulated 3D radiation patterns close to these peak resonance frequencies are presented in Figure 4. As seen in Figures 4(a) and 4(b), the radiation patterns at 2.41 GHz and 5.92 GHz resemble a doughnut, comparable to a dipole pattern. The patterns create humps in the up-right directions (gain increasing) and are squashed in the negative z-direction when at 8.86, 10.91, 18.33, and 22.98 GHz, respectively, as shown in Figures 4(c)–4(f). It is also noticed that the patterns on the H-plane are almost omnidirectional at all frequencies.
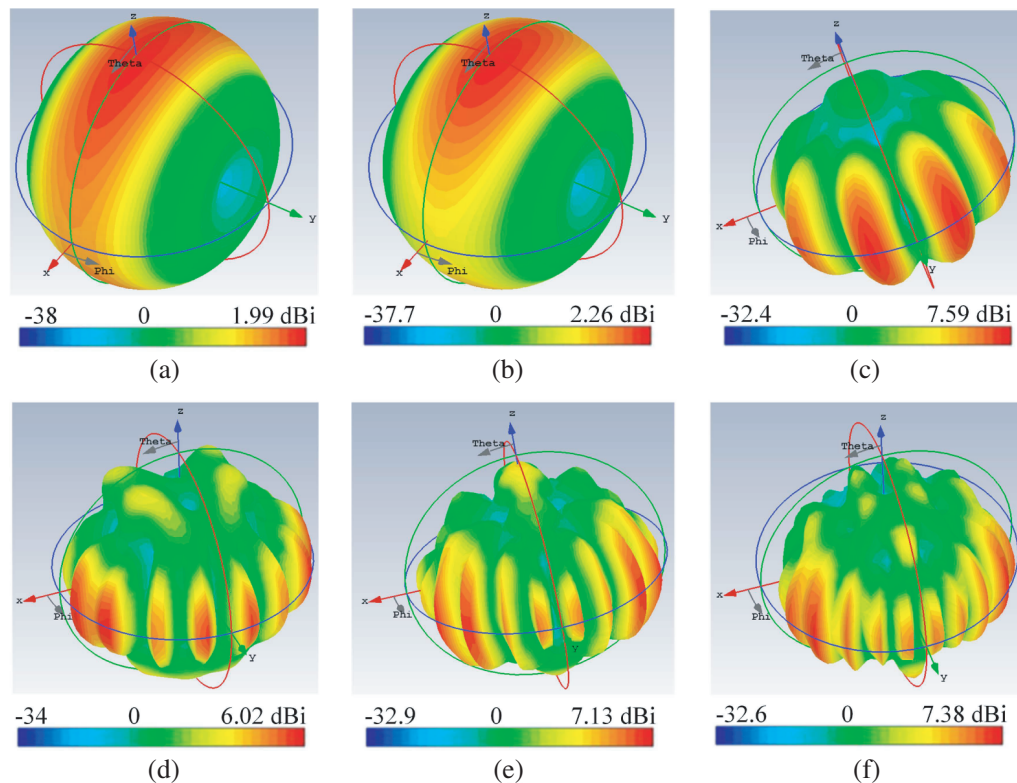

Figure 4. Simulated 3D radiation patterns of the proposed antenna for (a) 2.41 GHz, (b) 5.92 GHz, (c) 8.86 GHz, (d) 10.91 GHz, (e) 18.33 GHz, and (f) 22.98 GHz.

3. PARAMETRIC AND MATCHING ANALYSIS

The proposed antenna mirroring performance is sensitive to changes in geometrical parameters because of its compact size. An essential parametric analysis has been focused in order to show how important parameters affect an antenna's S_{11} performance across the desired operational SWB from 1.90 to 28.06 GHz (174.61%) with the impedance matching of 50 Ω feedline. The studies are carried out by keeping all other parameters constant and choosing the parameters outer radius r_2 of the radiator and width w_g and length l_g of the CPW-fed symmetric defective ground plane.

3.1. Effect of Outer Radius r_2

The effects of changes in outer radius r_2 on the effectiveness of the proposed antenna are shown in Figure 5(a). Radius r_2 is changed for this analysis in steps of 0.2 mm from 16.8 to 17.4 mm. According to this analysis, $r_2 = 17.2$ mm is the optimum option to cover the frequency range of 1.90 to 28.06 GHz. Figure 5(a) indicates that when r_2 decreases, the upper band frequency will shift toward the lower frequency. The operating frequencies of the proposed antenna have also been seen to somewhat shift
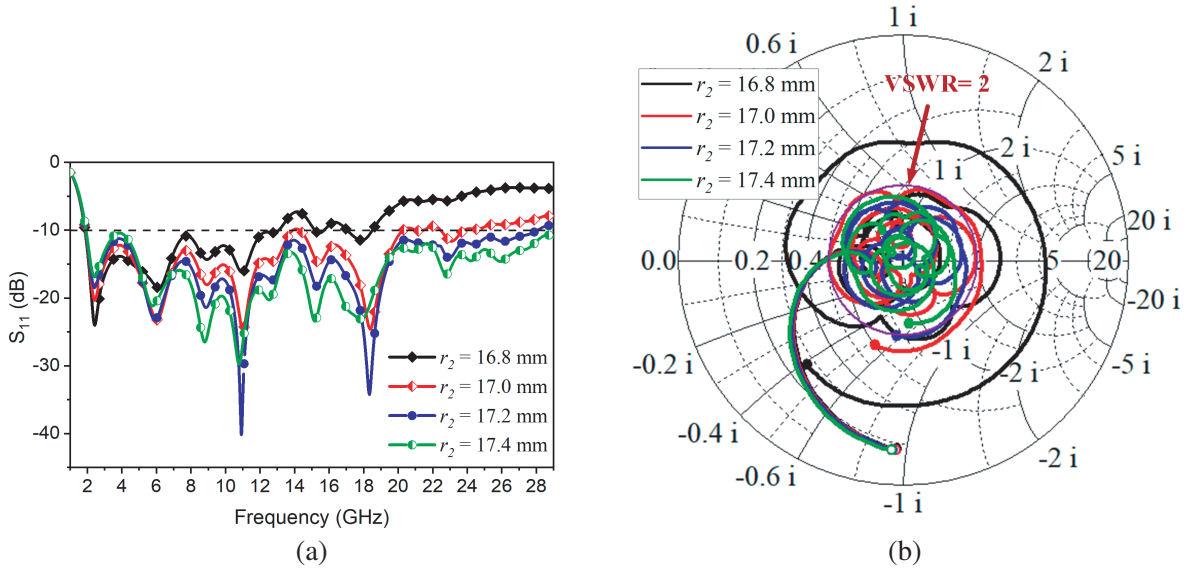
Figure 5. (a) S_{11} for various r_2 values and (b) corresponding impedance matching Smith chart of the proposed antenna.

to the left and right sides of the frequency spectrum as a result of the respective decrease and increase in r_2. As a result, the proposed antenna can additionally use r_2 as a frequency tuning parameter. The outer radius r_2 of 17.2 mm is selected as the ideal value since it satisfies the anticipated bandwidth need, impedance matching, and retains a low profile for the proposed design.

3.2. Effect of Ground Plane Width w_g

Figure 6(a) illustrates how rectangular ground plane width w_g affects the proposed antenna's IBW. The width w_g is varied for this analysis from 20.1 to 21.6 mm. The frequency range between 1.90 and 28.06 GHz can be properly covered by the $w_g = 21.1$ mm, which is the best-optimized value. According
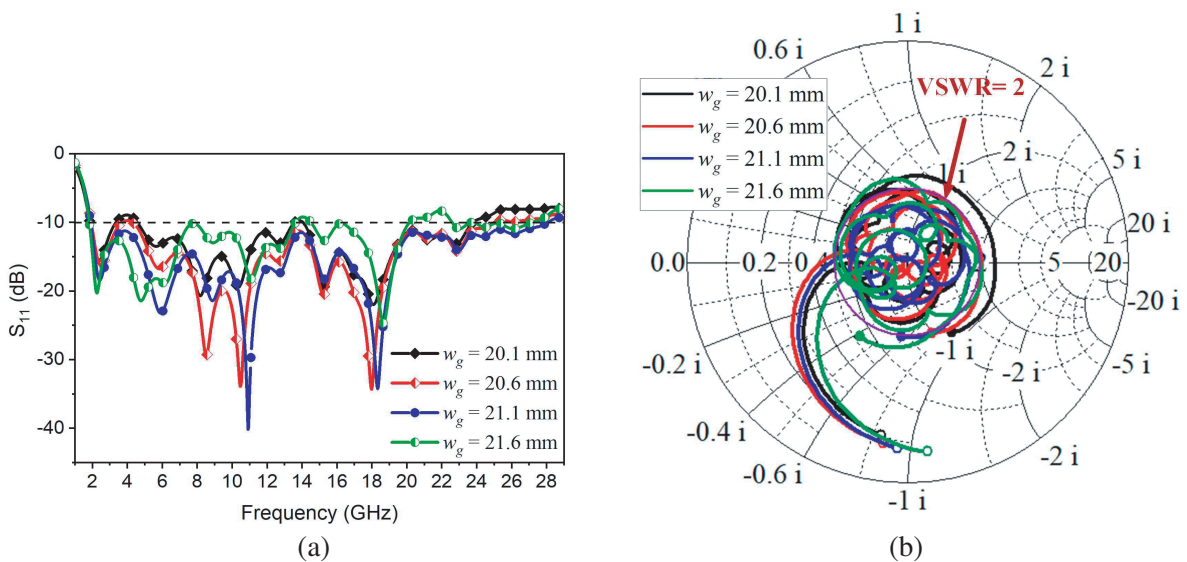

Figure 6. (a) S_{11} for various w_g values and (b) corresponding impedance matching Smith chart of the proposed antenna.

to Figure 6(a), the resonance shifts from the lower and upper-frequency spectrum when width w_g increases or decreases from 20.1 mm to 21.6 mm in step increments of 0.5 mm. The increase in width w_g also led to a little shift in the operating frequencies toward the right side of the frequency spectrum. Due to the achievement of the necessary impedance bandwidth with resonance 1.90–28.06 GHz (174.61%), the w_g of 21.1 mm is selected as the optimal value in this case.

3.3. Effect of Ground Plane Length l_g

The simulated S_{11} performance with different ground lengths l_g is shown in Figure 7(a). The S_{11} results show that the proposed antenna's CPW-fed ground length l_g has an impact on both the upper and lower side-band frequencies. More specifically, a decrease in length l_g below 7.7 mm affects upper side band bandwidth and return loss performance. The defective ground plane's inductance L_{eq} increases with increasing length l_g. Therefore, this causes the propagation constant β (i.e., $\beta \propto \sqrt{L_{eq}}$) to increase and as a result, reduces the effective dielectric constant $\sqrt{\epsilon_{eff}} = \beta/L_{eq}$. When the length of the defective ground plane is kept constant, the guided wavelength $\lambda_g = \lambda_0/\sqrt{\epsilon_{eff}}$ meets the resonance requirement [16, 21]. Figure at $l_g = 7.7$ mm illustrates that the proposed antenna exhibits a very wider bandwidth. It is also seen that the wideband performance decreases with a further increase in length l_g from 7.7 to 8.1 mm due to lower sideband effects.
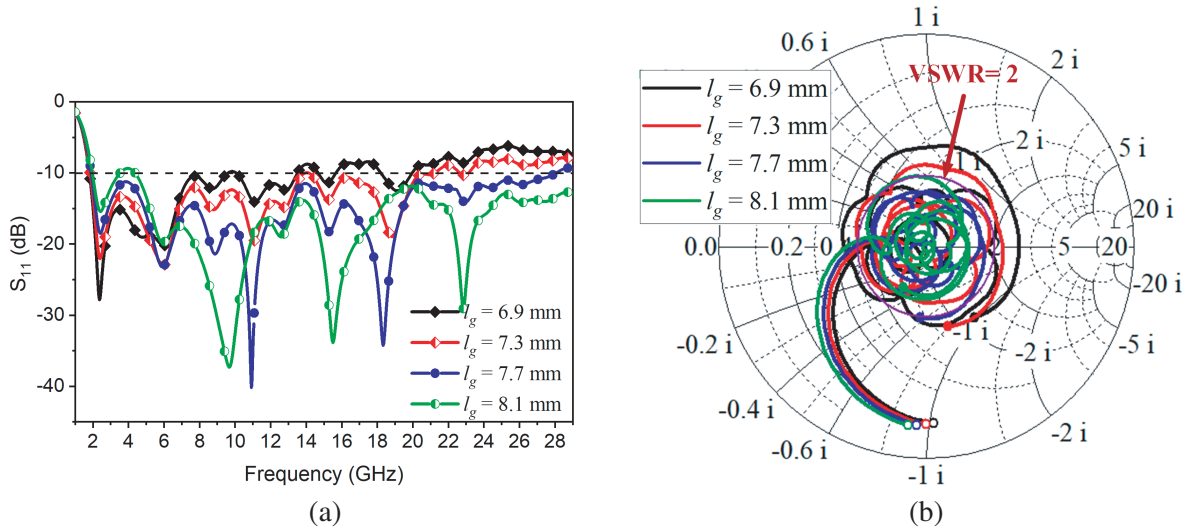

Figure 7. (a) S_{11} for various l_g values and (b) corresponding impedance matching Smith chart of the proposed antenna.

3.4. Effect of Ground Plane Partially Circular Slit Gap g

The effect of the proposed antenna's IBW on the rectangular ground plane partially circular slits gap g is shown in Figure 8(a). The gap g is adjusted in steps of 0.5 mm in the range of 0.8 to 2.3 mm. The best-optimized value of gap $g = 1.8$ mm, can properly cover the frequency from 1.90–28.06 GHz (174.61%). Figure 8(a) shows that the resonance shifts from the lower to the upper frequency spectrum as a result of a decrease in IBW when the slit gap g increases from 0.8 mm to 2.3 mm.

3.5. Effect of Elliptical-Shaped Slot Major Axes e_{m1}

The proposed antenna IBW relationship to the elliptical-shaped slot major axis length e_{m1} is shown in Figure 9(a). The major axis length e_{m1} is adjusted in steps of 0.5 mm in the range of 1.8 to 3.3 mm. The optimized value for e_{m1} is 2.8 mm, which can cover the frequency range between 1.90 and 28.06 GHz. Figure 9(a) shows that when length e_{m1} changes from 1.8 mm to 3.3 mm, the resonance shifts from the
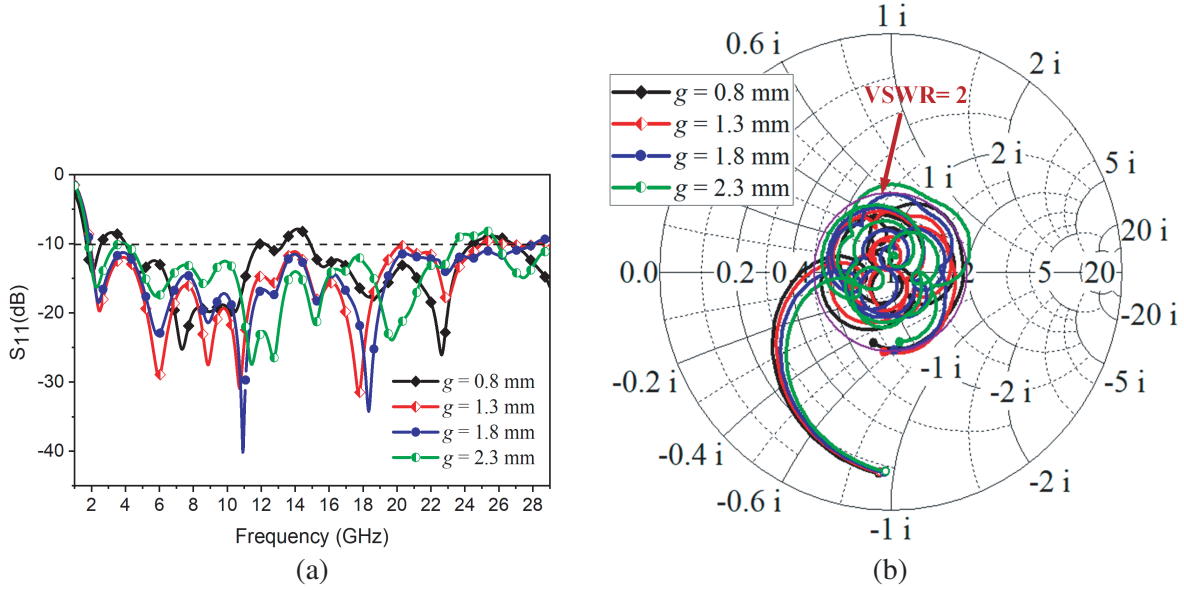
Figure 8. (a) S_{11} for various gap g values and (b) corresponding impedance matching Smith chart of the proposed antenna.
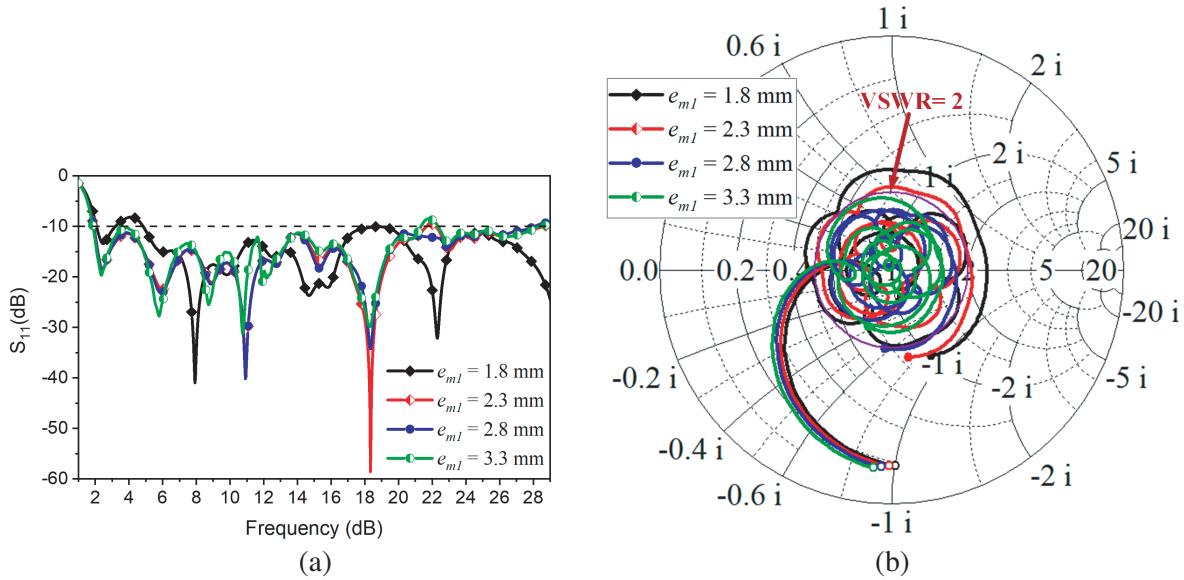

Figure 9. (a) S_{11} for various e_{m1} values and (b) corresponding impedance matching Smith chart of the proposed antenna.

lower to the upper frequency spectrum. Additionally, it is seen that lower and upper sideband effects cause the wideband performance to decrease as major axis length e_{m1} is increased further from 1.8 to 2.8 mm.

The Smith charts produced by CST Microwave Studio parametric analysis were used to match the impedance performance of the proposed antenna. The S_{11} variation with r_2, w_g, l_g, g, and e_{m1} are depicted in Figures 5(b), 6(b), 7(b), 8(b) and 9(b), respectively. The Smith curve's loop is seen to get smaller as r_2 increases, but as r_2 increases further to 17.4 mm the Smith curve outside the voltage standing wave ratio (VSWR $\approx$ 2) circle. The loop is rotating clockwise at the same time. At a frequency close to 28 GHz, an antenna becomes more capacitive. Higher frequencies deviate from the VSWR $\approx$ 2

circle while lower frequencies are inside it. Figure 6(b) depicts the parametric variation of w_g, and similar effects are seen there. It is evident that when w_g increases, the antenna shifts upward in the frequency range.

Next, we take l_g addition into account. The inclusion of l_g, g, and e_{m1} causes the loop of the Smith curve, as illustrated in Figures 7(b), 8(b), and 9(b) to extend. As a result, S_{11} values approximately below 4 GHz have moved outside the VSWR ≈ 2 circle. Based on the knowledge learned through parametric research, the actions listed below were taken to regain the matching.

- To rotate the loop and achieve satisfactory matching at the lower end of the band, the outer radius r_2 is extended by 0.2 mm.
- Next, the width w_g is increased by 0.5 mm to rotate the loop and prevent good matching from being seen at both the lower and upper ends of the band.
- Like w_g, length l_g, gap g, and major axis length e_{m1} are subsequently increased by 0.4, 0.5, and 0.5 mm to rotate the loop, preventing good matching from being seen at both the lower and upper ends of the band.

Following these three stages, it is found that the antenna matched VSWR ≈ 2 from 1.91 to 28 GHz. Figure 10 additionally displays the matched Smith curve. The IBW behavior in Figure 10 shows that the proposed antenna provides the best impedance match with an IBW of 174.61%. The simulated peak resonant frequencies and associated impedance are shown in Table 2.
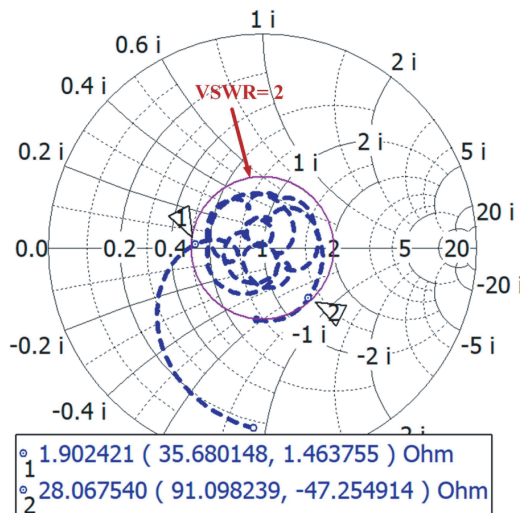

Figure 10. Proposed antenna simulated result of the impedance matching.

Table 2. Simulated peak resonant frequencies and corresponding impedances of the proposed antenna.

Resonant	Simulation frequency (GHz)	Impedance (Ω)
First	$f_{rp1} = 2.41$	$Z_1(f_{rp1}) = 53.780 - j2.073$
Second	$f_{rp2} = 5.92$	$Z_1(f_{rp2}) = 77.413 - j3.996$
Third	$f_{rp3} = 8.86$	$Z_1(f_{rp3}) = 59.177 + j6.041$
Fourth	$f_{rp4} = 10.91$	$Z_1(f_{rp4}) = 68.180 + j1.338$
Fifth	$f_{rp5} = 15.30$	$Z_1(f_{rp5}) = 82.225 - j11.913$
Sixth	$f_{rp6} = 18.33$	$Z_1(f_{rp6}) = 68.862 + j2.568$
Seventh	$f_{rp7} = 22.98$	$Z_1(f_{rp7}) = 56.062 + j21.669$

4. SIMULATION AND MEASUREMENT RESULTS

To verify the simulated results, an optimal fabricated prototype of the presented SWB elliptical slot monopole antenna is fabricated and tested. A vector network analyzer (VNA) (Rohde and Schwarz ZVA24) measures the performance of the proposed antenna. Figure 11 shows the prototype antenna and the measurements set up taken for the validation. In an anechoic chamber (size: $6 \times 4 \times 6\,\mathrm{m}^3$), the antenna measuring environment is used to measure the 1–28 GHz band's reflection coefficient S_{11}, peak gain, efficiency, and radiation patterns.
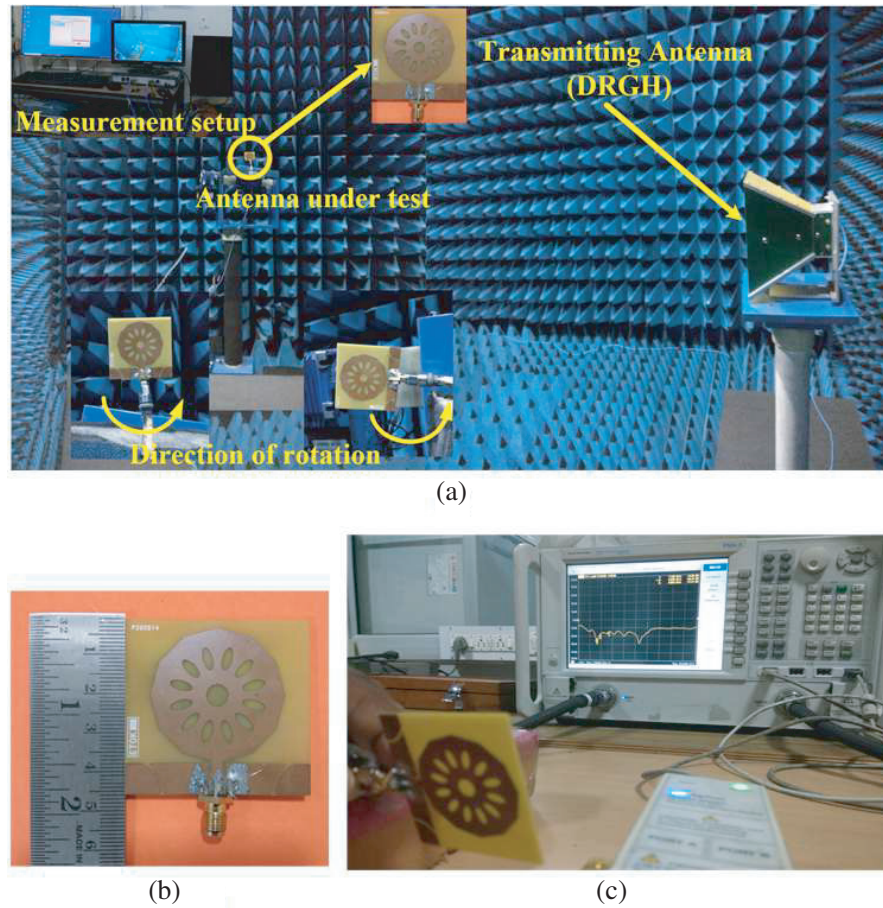

Figure 11. (a) Measurement setup inside an anechoic chamber, (b) photograph of the prototype antenna, and (c) using VNA.

4.1. Reflection Coefficient S_{11}

Figure 12 shows the proposed antenna measured and simulated reflection coefficient S_{11} parameters. A photograph of the fabricated prototype antenna can be seen in the inset figure. The measured result shows a very wider IBW from 1.613–26.357 GHz (176.93%) whereas the simulated from 1.90–28.06 GHz (174.61%) with a high bandwidth ratio of approximately 16.34 : 1. For the entire operating band, the CST simulator's simulated results and measured results agree very closely. The SMA connector and fabrication tolerance are mostly attributed to the small variation in the lower and higher sideband.
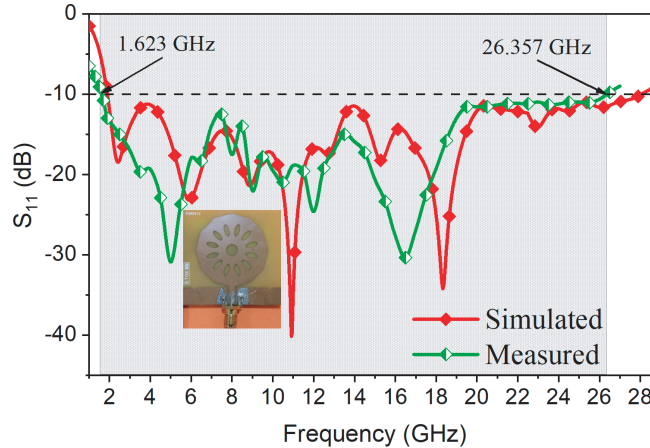
Figure 12. Measured and simulated S_{11} performance of the proposed antenna.

4.2. Gain and Radiation Efficiency

Measured and simulated peak gains of the proposed antenna are shown in Figure 13(a). The peak gains measured are 2.35, 7.32, 7.12, and 6.36 dBi at 4.85, 13.54, 16.52, and 20.57 GHz, respectively. It can be shown that the measured peak gain closely approaches the simulation's outcomes across the entire operating band. The peak gain varies from 0.4 to 7.32 dBi for a frequency up to 26.5 GHz.
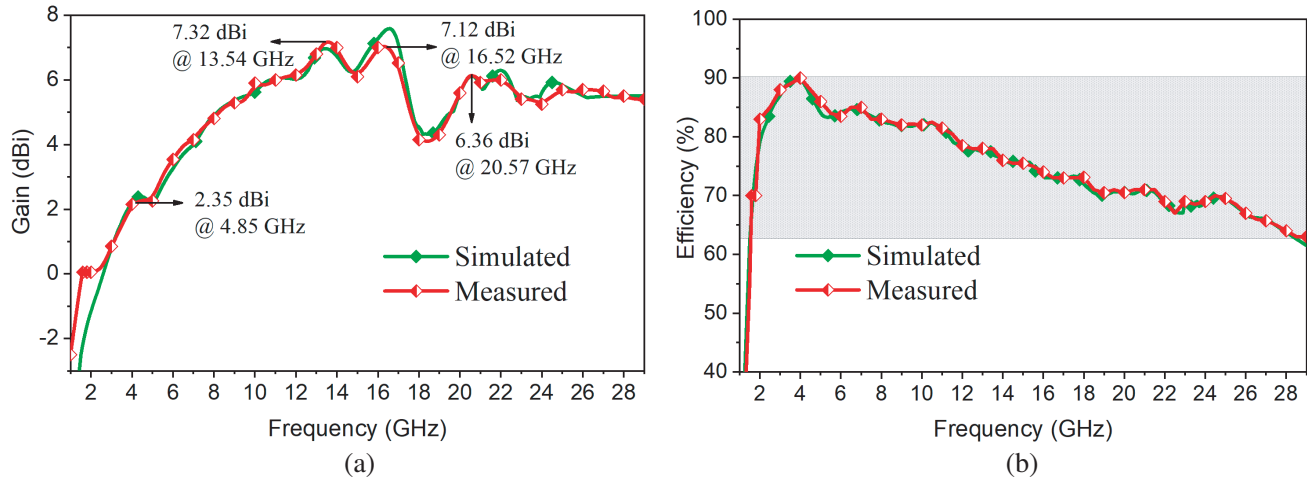

Figure 13. Measured and simulated the proposed antenna. (a) Peak gain and (b) efficiency.

The gain $G(\theta, \phi)$, radiation intensity, and reflection coefficient S_{11} of the proposed antenna are measured first to determine the radiation efficiency. The radiation intensity is used to automatically calculate the directivity $D(\theta, \phi)$. The equation below is used to calculate the antenna efficiency (η) using the above parameters [22]:

$$\eta = \frac{G(\theta, \phi)}{D(\theta, \phi)} \left(1 - |S_{11}|^2\right) \tag{5}$$

Figure 13(b) shows the measured and simulated radiation efficiency performance. Within the operational band, measured efficiency ranges from 73 to 90.2% between 1.6 and 26.5 GHz. Due to manufacturing tolerance, there is a minor difference between the measurement and the simulated result and acceptable radiation efficiency.
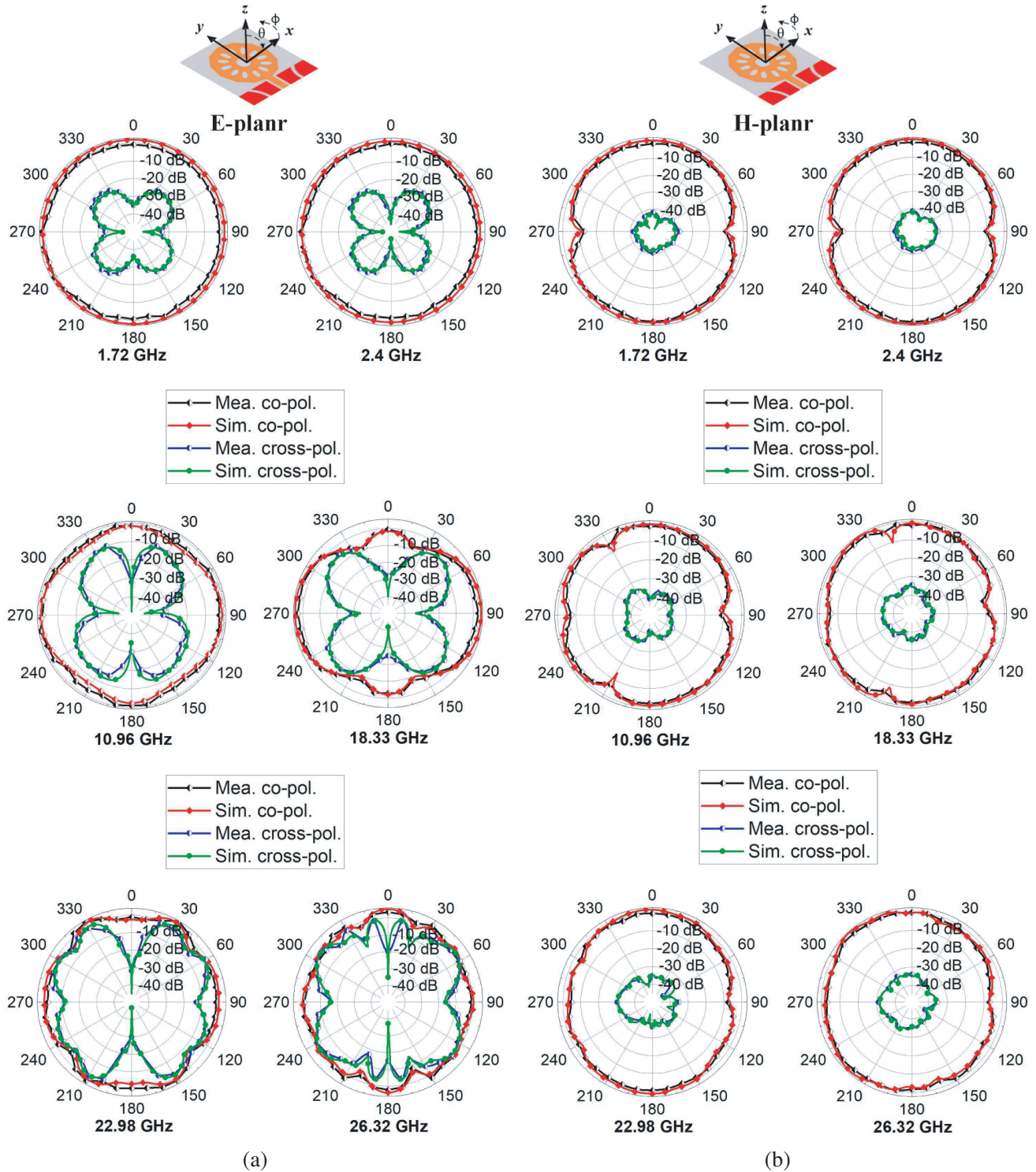
Figure 14. Measured and simulated radiation patterns of the proposed antenna at 1.72, 2.4, 10.96, 18.33, 22.98, and 26.32 GHz for (a) *E*-plane (*yoz* plane) and (b) *H*-plane (*xoz* plane).

4.3. Radiation Performance

Figures 14(a) and 14(b) show the simulated and measured radiation patterns in the E-plane (yoz plane) and H-plane (xoz plane) for frequencies of 1.71, 2.4, 10.96, 18.33, 22.98, and 26.32 GHz, respectively. The antenna operates quite similarly to an elliptical slot monopole antenna in the lower and medium frequency bands when seen as a whole from these radiation patterns. The cross-polarization levels of the H-plane radiation pattern are significantly reduced and well maintained at higher frequencies, while the cross-polarization levels of the E-plane radiation pattern increased. However, the seriously unequal phase distribution of the antenna aperture, increasing magnitudes of higher order modes, and measurement error are to attribute for the slightly distorted radiation patterns in the higher frequency in the E-plane at 18.33, 22.98, and 26.32 GHz [23]. The cross-polarization levels at the proposed antenna boresight are approximately -39 dBi lower than the co-polarization levels for the H-plane in all circumstances. The results of the measurements demonstrate that the proposed antenna radiates in the UWB band with consistent and nearly omnidirectional patterns.

4.4. Time Domain Analysis

The time-domain and frequency-domain analyses are of equal importance to study the time-domain characteristics of the designed antenna while the antenna transmits or receives the signal. The time domain analysis of the designed antenna is carried out by keeping two similar antennas face-to-face at a distance of 35 cm from each other. A Gaussian pulse, having a center frequency of 13.08 GHz is transmitted and received by the transceiver antenna structures. Figure 15(a) demonstrates the incident and received pulses and Figure 15(b) variation of the group delay over the frequency.
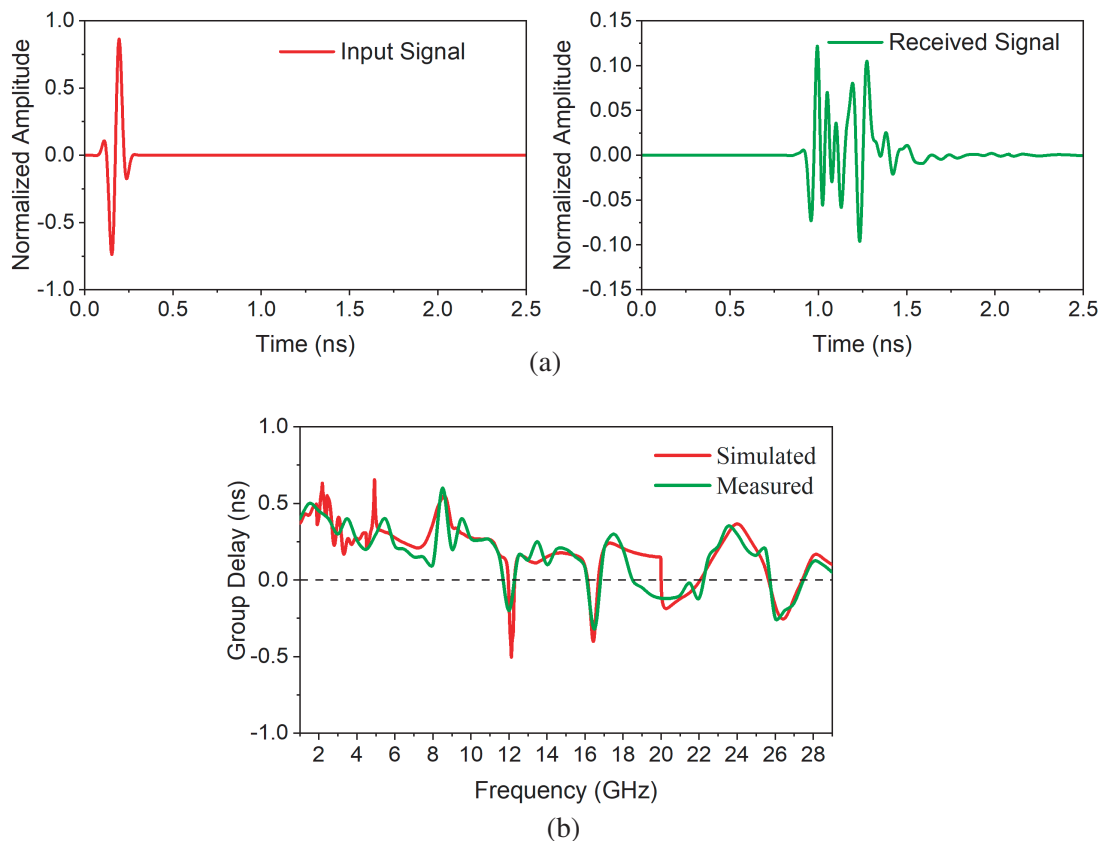

Figure 15. Time domain analysis of the proposed antenna. (a) Normalized amplitude of the input and received signals and (b) group delay.

The pulse fidelity factor is calculated when the transmitting and receiving antennas are kept face-to-face at some distance [24, 25]. To evaluate the degree of waveform distortion, the correlation factor is calculated between the input signal $S_1(t)$ and the output signal $S_2(t)$, and the correlation factor (ρ) is expressed below:

$$\rho = \max \left\{ \frac{\int S_1(t)S_2(t-\tau)\,dt}{\sqrt{S_1^2(t)}\sqrt{S_2^2(t)}\,dt} \right\} \tag{6}$$

where τ is the delay. It is observed that the pulse-preserving capability is the best when the orientation of the transmitting-receiving antennas and the system is face-to-face with each other, and the correlation factor is found to be 0.9315. Group delay is related to the performance of the antenna gain and mathematically calculated by using the group delay equation [26]. It is observed that the group delay is almost constant and that variation less than 1 ns across the entire operating band.

The performances (antenna type, substrate, dimension, frequency range, IBW (% BW), peak gain, H-plane cross-polarization, and radiation pattern) of the proposed antenna are compared with the recently published progressive state-of-the-art and displayed in Table 3 to validate their potency. It is noteworthy that the proposed antenna outperforms the ones that have been published in terms of radiation performance, cost-effectiveness, and small size.

Table 3. Comparison of the proposed antenna with other recently reported antennas.

Ref.	Type (Antenna)	Substrate	Dimension (mm³)	Freq. (GHz)	IBW (%)	PG (dBi)	Hx-pol. (dBi)	Radiation pattern
5	Slot antenna	RT Duroid Roger 5880	$0.24 \times 0.32 \times 0.016\lambda_l^3$	3.1–10.9	111.42	-1–4	N. A.	N. A.
7	Monopole	RT Duroid (6010LM)	$0.35 \times 0.35 \times 0.006\lambda_l^3$	3.1–11	112.05	2.1–5.6	N. A.	Omni-directional
9	Monopole array	Rogers (RO4003)	$0.36 \times 0.30 \times 0.004\lambda_l^3$	1.8–7.3	120.9	4.9-11.2	20	N. A.
10	Slot antenna	FR-4	$0.24 \times 0.29 \times 0.007\lambda_l^3$	2.9–11.8	121	2–6	20	N. A.
11	Fractal	Rogers (TMM)	$2 \times 2 \times 0.05\lambda_l^3$	10–50	133.33	N. A.	N. A.	N. A.
13	Slot antenna	FR-4	$0.80 \times 0.80 \times 0.009\lambda_l^3$	2.83–18.2	146	2–6.5	35	Omni-directional
14	Slot antenna	Rogers (RO4003)	$0.88 \times 0.88 \times 0.006\lambda_l^3$	3.7–19.3	135	-1–4.5	N. A.	N. A.
16	Slot antenna	RT Duroid Roger 5880	$0.23 \times 0.22 \times 0.004\lambda_l^3$	1.55–16.95	166.51	2–8.3	20	Omni-directional
17	Monopole	FR-4	$0.37 \times 0.17 \times 0.007\lambda_l^3$	1.44–18.8	172	1–7	N. A.	N. A.
Work	Slot antenna	FR-4	$0.23 \times 0.25 \times 0.004\lambda_l^3$	1.61–26.35	176.93	0.4–7.32	39	Omni-directional

IBW: Impedance bandwidth. PG: Peak gain. NA: Not available. Hx-pol.: H-plane cross-polarization.

Following are some notable and significant characteristics of the proposed antenna based on this performance comparison:

- In comparison to [5, 7, 9–11, 13, 14, 17], the proposed antenna is compact and has smaller dimensions.

- The proposed antenna doesn't need an expensive substrate, unlike [5, 7, 9, 11, 14, 16].
- The proposed antenna is much thinner (low in profile) than [5, 7, 10, 11, 13, 14, 17] and can be employed in next-generation wireless devices (with slim characteristics).
- In comparison to [5, 7, 10, 13, 14, 17], the proposed antenna has a higher gain.
- The proposed antenna is cost-effective because, in contrast to [5, 7, 9, 11, 14, 16], it does not require an expensive RT-Duroid substrate and reactive components or both. It also has lower fabrication costs because of its small size, in contrast to [5, 7, 9–11, 13, 14, 17].

Additionally, all of the stated varieties have high cross-polarization levels, whereas the proposed antenna has a relatively low $-39\,\text{dBi}$. The proposed antenna will be therefore a strong option for wireless applications when all of its performance is taken into account.

5. CONCLUSION

The purpose of this work is to explain a compact CPW-fed SWB elliptical slot monopole (ESM) antenna with a defective ground plane for enhanced IBW. The defective ground plane, which consists of two partially circular slits in the ground plane and 12 elliptical-shaped slots on the radiator, provides a very wide IBW and low cross-polarization levels. Due to a defective ground plane, the intended ESM antenna has an overall size of $44.5 \times 47.20 \times 0.8\,\text{mm}^3$. The measured S_{11} result from 1.613 to 26.357 GHz (176.93%) is achieved. The antenna has nearly omnidirectional radiation patterns, a reasonable gain, low cross-polarization levels, and a tolerable radiation efficiency which will be a strong option for wireless applications.

ACKNOWLEDGMENT

REFERENCES

1. Molisch, A. F., K. Balakrishnan, D. Cassioli, C.-C. Chong, S. Emami, A. Fort, J. Karedal, J. Kunisch, H. Schanntz, and K. Siwiak, "A comprehensive model for ultrawideband propagation channels," *Proc. IEEE Global Telecommun. Conf. (GLOBECOM)*, 3648–3653, 2005.
2. Porcino, D. and W. Hirt, "Ultra-wideband radio technology: Potential and challenges ahead," *IEEE Commun. Mag.*, 66–74, Jul. 2003.
3. *FCC First Report and Order on Ultra-Wideband Technology*, document FCC 02-48, Feb. 2002.
4. Chiu, S. C. and S. Y. Chen, "Miniaturization of CPW-fed slot antenna using a pair of interdigital capacitors," *in Proc. IEEE Antennas Propag. Soc. Int. Symp., (APSURSI)*, 1380–1381, Orlando, FL, USA, Jul. 2013.
5. Orazi, H. and H. Soleiman, "Miniaturisation of UWB triangular slot antenna by the use of DRAF," *IET Microw. Antennas & Propag.*, Vol. 11, No. 4, 450–456, Feb. 2017.
6. Sallam, M. O., S. M. Kandil, V. Volski, G. A. E. Vandenbosch, and E. A. Soliman, "Wideband CPW-fed flexible bow-tie slot antenna for WLAN/WiMAX systems," *IEEE Trans. Antennas Propag.*, Vol. 65, No. 8, 4274–4277, Aug. 2017.
7. Safia, O. A., M. Nedil, L. Talbi, and K. Hettak, "Coplanar waveguide-fed rose-curve shape UWB monopole antenna with dual-notch characteristics," *IET Microw. Antennas & Propag.*, Vol. 12, No. 7, 1112–1119, Jan. 2018.
8. Maity, B. and S. K. Nayak, "Compact quad-band CP series-fed circular slit microstrip array antenna using machine learning," *IEEE Access*, Vol. 10, 116650–116661, Aug. 2022.
9. Xu, R., Z. Shen, and S. S. Gao, "Compact-size ultra-wideband circularly polarized antenna with stable gain and radiation pattern,," *IEEE Trans. Antennas Propag.*, Vol. 70, No. 2, 943–952, Sept. 2022.

10. Yang, Y., Z. Zhao, X. Ding, Z. Nie, and Q.-H. Liu, "Compact UWB slot antenna utilizing traveling-wave mode based on slot line transitions," *IEEE Trans. Antennas Propag.*, Vol. 67, No. 1, 140–150, Jan. 2019.

11. Azari, A., "A new super wideband fractal microstrip antenna," *IEEE Trans. Antennas Propag.*, Vol. 59, No. 5, 1724–1727, May 2011.

12. Fang, X., G. Wen, D. Inserra, Y. Huang, and J. Li, "Compact wideband CPW-fed meandered-slot antenna with slotted Y-shaped central element for Wi-Fi, WiMAX, and 5G applications," *IEEE Trans. Antennas Propag.*, Vol. 66, No. 12, 7395–7399, Dec. 2018.

13. Dastranj, A. and H. Abiri, "Bandwidth enhancement of printed E-shaped slot antennas fed by CPW and microstrip line," *IEEE Trans. Antennas Propag.*, Vol. 58, No. 4, 1402–1407, Apr. 2010.

14. Moghadasi, M. N., A. Danideh, R. Sadeghifakhr, and M.-R. Azadi, "CPW-fed ultra wideband slot antenna with arc-shaped stub," *IET Microw. Antennas & Propag.*, Vol. 3, No. 4, 681–686, Sept. 2009.

15. Liu, H., S. Zhu, P. Wen, X. Xiao, W. Che, and X. Guan, "Flexible CPW-fed fishtail-shaped antenna for dual-band applications," *IEEE Antennas Wireless Propag. Lett.*, Vol. 13, 770–773, Apr. 2014.

16. Maity, B. and S. K. Nayak, "Design of compact CPW-fed symmetrical staircase-shaped UWB antenna using transmission line model," *Progress In Electromagnetics Research C*, Vol. 115, 187–203, Sept. 2021.

17. Chen, K.-R., C. Y. D. Sim, and J.-S. Row, "A compact monopole antenna for super wideband applications," *IEEE Antennas Wireless Propag. Lett.*, Vol. 10, 488–491, Apr. 2011.

18. Faisal, F., Y. Amin, Y. Cho, and H. Yoo, "Compact and flexible novel wideband flower-shaped CPW-fed antennas for high data wireless applications," *IEEE Trans. Antennas Propag.*, Vol. 67, No. 6, 4184–4188, Jun. 2019.

19. Balanis, C. A., *Antenna Theory Analysis and Design*, 2nd Edition, John Wiley & Sons, In INC Hoboken, 1997.

20. Vyas, K., G. Sanyal, A. K. Sharma, and P. K. Singhal, "Gain enhancement over a wideband in CPW-fed compact circular patch antenna," *Int. J. Microw. Wireless Technol.*, Vol. 6, No. 5, 497–503, Oct. 2014.

21. Zhang, L., Y.-C. Jiao, Y. Ding, B. Chen, and Z.-B. Weng, "CPW-fed broadband circularly polarized planar monopole antenna with improved ground plane structure," *IEEE Trans. Antennas Propag.*, Vol. 61, No. 9, 4824–4828, Sept. 2013.

22. Abutarboush, H. F., H. Nasif, R. Nilavalan, and S. W. Cheung, "Multiband and wideband monopole antenna for GSM900 and other wireless applications," *IEEE Antennas Wireless Propag. Lett.*, Vol. 11, 539–542, Apr. 2012.

23. Sze, J.-Y. and K.-L. Wong, "Bandwidth enhancement of a microstrip-line-fed printed wide-slot antenna," *IEEE Trans. Antennas Propag.*, Vol. 49, No. 7, 1020–1024, Jul. 2001.

24. Yang, Y. Y., Q.-X. Chu, and Z.-A. Zhe, "Time domain characteristics of band notched ultrawideband antenna," *IEEE Trans. Antennas Propag.*, Vol. 57, No. 10, 3426–3430, Oct. 2009.

25. Chen, Z. N. and M. Y. W. Chia, *Broadband Planar Antenna Design and Applications*, John Wiley & Sons., New York, NY, USA, 2006.

26. Wiesbeck, W., G. Adamiuk, and C. Sturm, "Basic properties and design principles of UWB antennas," *Proc. IEEE*, Vol. 97, No. 2, 372–385, Feb. 2009.